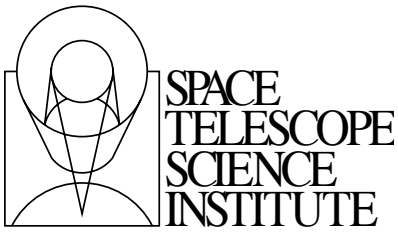

Operated for NASA by AURA

Instrument Science Report WFC 2013-09

WFC3/UVIS Bowtie Monitor

M. Bourque & S. Baggett
June 21, 2013

Abstract

We present the results of the WFC3/UVIS bowtie monitoring program based on data acquired during SMOV/Cycle 17 through current observations of Cycle 20, spanning all on-orbit data (June 2009 - June 2013). The bowtie program serves as a periodic monitor for intermittent low-level (up to ∼4%) detector hysteresis, i.e. a QE deficit across each UVIS CCD chip. A set of three internal flat fields is used to probe for hysteresis, neutralize any QE deficits via a saturated QE 'pinning' exposure, and assess the effectiveness of the hysteresis mitigation. Image ratios involving the flat fields before and after the saturating exposure indicate that hysteresis features (1) are detectable only in the first bowtie visit after UVIS anneal procedures wherein the detector is warmed then cooled back down to operating temperature and (2) are effectively suppressed at all times, ensuring that science observations are not compromised by QE offsets. For the first time on-orbit, a bowtie-shaped hysteresis pattern, for which the program is named, was observed following the August 2012 UVIS anneal; to date, this incident has been a one-time anomalous event on-orbit. A by-product of the bowtie monitoring data is the discovery of a slow decrease in flux level over time, currently about ∼0.19±0.01%/yr. Assuming the decline is due solely to the aging of the lamp, the lamp output is currently at ∼98% of its original level.

Introduction

The Wide Field Camera 3 (WFC3), installed during Servicing Mission 4 (SM4) in May 2009, is a fourth-generation imaging instrument on board HST and consists of two channels: UVIS (spanning

the ultraviolet and visible spectrum) and IR (spanning the infrared spectrum). During ground-based thermal vacuum tests of internal flat fields, the UVIS detector (which is comprised of two 2K x 4K e2v CCDs) was found to exhibit occasional low-level hysteresis, a quantum efficiency (QE) deficit across both chips (Baggett & Richardson, 2004). Due to the unique shape manifested in the flat field ratios, this feature was named the "bowtie" effect. At the nominal operating temperature of -83C, the feature was observed as a ∼0.1-0.2% up to ∼1% offset in a small percentage of the ground-based flat-field images, and reached a contrast of up to 5% at warmer temperatures (-50C). Furthermore, Collins et al. 2009 showed through lab tests on flight spare detectors at the Goddard Space Flight Center (GSFC) Detector Characterization Laboratory (DCL) that detector hysteresis (1) could be induced by power cycling the detector while cold or cooling the detector in the dark, (2) could be present as a global QE offset across the chip without a discernible pattern such as the 'bowtie', and (3) could be suppressed by filling charge traps with a saturated visible light (500-580nm) exposure at a level of several hundred thousand electrons per pixel, thereby 'pinning' the QE to its optimum level. The lab tests also showed that a sensitivity reduction of 0.10% occurs after a ten day period, implying that the hysteresis behavior can be effectively mitigated to extremely low levels by routine application of a QE 'pinning' exposure where the chip is saturated to at least ∼2-3 times full-well.

With this knowledge, a 'bowtie monitoring' calibration program was adopted to periodically check and correct for UVIS hysteresis, and has been in use since the initiation of WFC3/UVIS in-flight operations. Since SM4, the calibration program has been employed during every proposal cycle, including Servicing Mission Orbital Verification 4 (SMOV4) in which the instruments of HST underwent a series of on-orbit calibrations before science observing. In this paper, we will discuss the makeup of a single bowtie visit, specific features seen in the internal flat fields, an anomalous event in which a bowtie-shaped hysteresis appeared following the August 2012 anneal, and our estimates of the QE offset removal efficiency.

Observations

Each bowtie observation consists of a single continuous visit containing three internal flat field exposures, as outlined in Table 1: (1) an unsaturated image to provide a check for the presence of hysteresis features and/or global QE deficits, (2) a saturated image at a level of ∼9 times the full well amount to neutralize QE offsets (i.e. a 'pinning' exposure), and (3) an additional unsaturated image to provide an estimate of the QE offset removal efficiency. Figure 1 shows two typical hysteresis-free unsaturated flat fields from a bowtie visit before (left) and after (middle) the saturating exposure, as well as the ratio of these images, showing a case where no features are present. Each exposure is taken with the F475X filter, chosen for its (1) high throughput, (2) 700nm bandpass, which is known to mitigate QE offsets, and (3) position within a lower priority filter wheel. Images are full-frame, four-amp readouts and are 3X3 binned so as to minimize data volume and overhead; each visit requires only ∼360 seconds of telescope time, not including dump time.

Exposure	Type	Filter	Exposure Time (s)
1	TUNGSTEN	F475X	1.0
2	TUNGSTEN	F475X	200.0
3	TUNGSTEN	F475X	1.0

Table 1: *Observational parameters for a single bowtie visit. Exposure 1 is unsaturated and used as a check for bowtie or global hysteresis features, exposure 2 is the saturated, neutralizing exposure that mitigates QE offsets, and exposure 3 is unsaturated as to provide a estimate for the mitigation efficiency.*

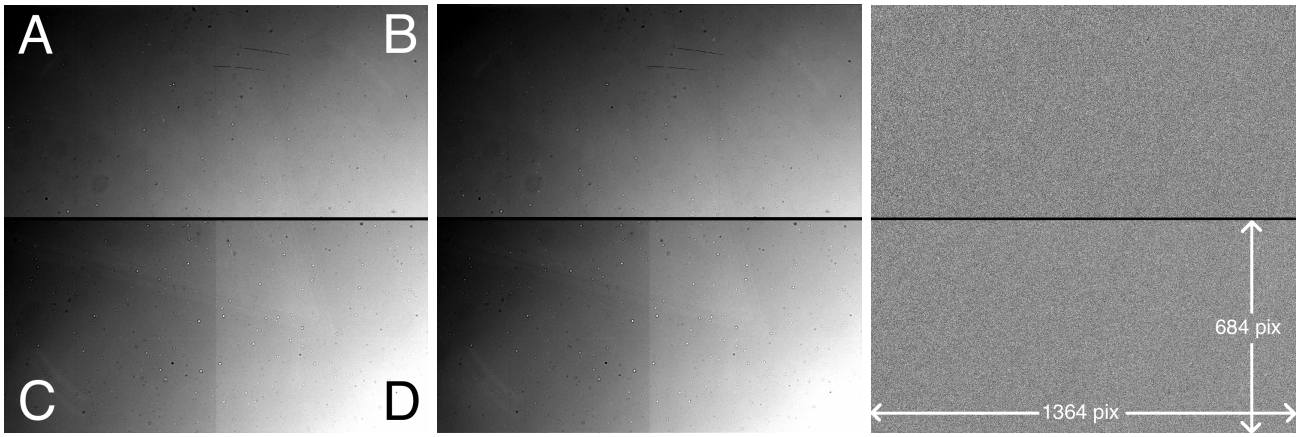

Fig. 1.—*Two typical UVIS F475X internal flat fields that make up the first and third exposure of a bowtie visit: An unsaturated exposure to check for hysteresis features (left, stretched to +/-20%), and another unsaturated exposure (middle, stretched to +/-20%) used to estimate the hysteresis neutralization efficiency of the 'pinning' exposure. The right panel shows the ratio of the two unsaturated flat fields (stretched to +/-7%). All images are 3X3 binned. Chip 1 is shown in the top panel while chip 2 is displayed in the bottom. Amps A, B, C, and D are labeled in the left image and image dimensions are labeled in the right image for reference.*

Collins et al. 2009 show that a 'pinning overshoot' can occur causing short-term detector QE instability wherein the detector sensitivity is greater immediately after the QE neutralizing exposure relative to the sensitivity measured 1-2 hours later. The rapidly-decaying overshoot (QE ∼1% high after 30 minutes, ∼0.5% high after 45 minutes) is caused by detector saturation combined with high count rates. A 2% overshoot occurred in DCL tests when (1) the detector was saturated to 7 times the full-well amount or beyond and (2) the lamp flux reached ∼6100e-/second, resulting in QE instability lasting roughly two hours (Figure 5, Collins et al. 2009). For this reason, the QE 'pinning' exposures for bowtie observations are obtained with count rates of ∼3000 e-/second, which is safely below the overshoot level. Based on these DCL results, it is conceivable that a highly saturating science observation can cause local QE instability for time periods on the order of 1-2 hours. However, there has been no evidence of a QE overshoot occurring for on-orbit bowtie or science data.

Program	Type	Cycle	Date Range	PI	Cadence
11808	Bowtie Monitor	SMOV/17	Jun 11 2009 - Aug 9 2009	J. MacKenty	Twice Daily
11908	Bowtie Monitor	17	Aug 10 2009 - Oct 5 2010	S. Baggett	Daily
11909	UVIS Anneal	17	Aug 21 2009 - Oct 15 2010	S. Baggett	Monthly
12343	UVIS Anneal	18	Nov 14 2010 - Sep 18 2011	S. Baggett	Monthly
12344	Bowtie Monitor	18	Oct 5 2010 - Oct 16 2011	T. Borders	Every 3rd Day
12687	UVIS Anneal	19	Oct 15 2011 - Sep 11 2011	S. Baggett	Monthly
12688	Bowtie Monitor	19	Oct 19 2011 - Oct 10 2012	T. Borders	Every 3rd Day
13104	Bowtie Monitor	19	Oct 13 2012 - Nov 6 2012	M. Bourque	Every 3rd Day
13071	UVIS Anneal	20	Nov 08 2012 - Oct 14 2013	S. Baggett	Monthly
13072	Bowtie Monitor	20	Nov 9 2012 - Aug 13 2013	M. Bourque	Every 3rd Day

Table 2: *WFC3/UVIS bowtie monitor and UVIS anneal program information.*

Observations were performed through the programs listed in Table 2 and were acquired through two different types: (1) the UVIS anneal and (2) the bowtie monitor. UVIS anneals, in which the detector is warmed up to ∼20C to restore hot pixels to normal levels, are always followed by a bowtie visit to correct for the hysteresis introduced during the cooldown procedure which follows the anneal. In addition, observations from the bowtie monitor check and correct for any intermittent hysteresis that appears between anneal cycles, though no evidence for this has been seen. Bowtie data were acquired at a faster cadence (two visits per day) during SMOV testing and cycle 17 as a conservative measure to mitigate hysteresis, but have since been reduced to a lower (but still conservative) cadence (one visit every three days).

Analysis

Image ratios involving the unsaturated exposures of the bowtie visit are created in an effort to uncover faint (<1%) features caused by hysteresis in the internal flat fields. These ratios are: (1) The first bowtie exposure to a 'reference image' (i.e. a hysteresis-free unsaturated internal flat field that is consistently used in comparisons to later data), (2) the first bowtie exposure to the third bowtie exposure, and (3) the third bowtie exposure to a reference image. iac702kkq_flt.fits and iac702kmq_flt.fits, which were obtained on 06/12/2009 (day 2) as the first and third bowtie image in Visit 02 of program 11808, were used as the reference images in this analysis. The image ratios are examined visually and by plotting the ratio's median values versus time (as will be discussed later). Here we discuss some features that appear in many of the image ratios as well as an anomalous case wherein the bowtie-shaped feature appeared on-orbit.

Nominal Ratio Features

There exist several recurring internal flat field features that are unrelated to hysteresis and appear before and after the QE 'pinning' exposure. These divide out in the image 1 /image 3 ratio but do not divide out in the image 1 to reference image ratios. One such feature is shown in Figure 2, seen as ∼70 pixel-wide dimples in the image 1/reference image ratio. This feature occurs because filter wheel 10, which houses the F475X filter, occasionally does not land on precisely the same position between moves. These features occur at levels of ±1% or less relative to surrounding pixels. The ∼70 pixel offset is consistent with the offset of 1 wheel step (0.5 degrees) from the nominal position. These 1-step offsets, however, do not impact external science observations; the features appear prominently in the internal flat fields as a result of the highly collimated beam inherent to only the internal calibration subsystem (Baggett and Borders, 2010).

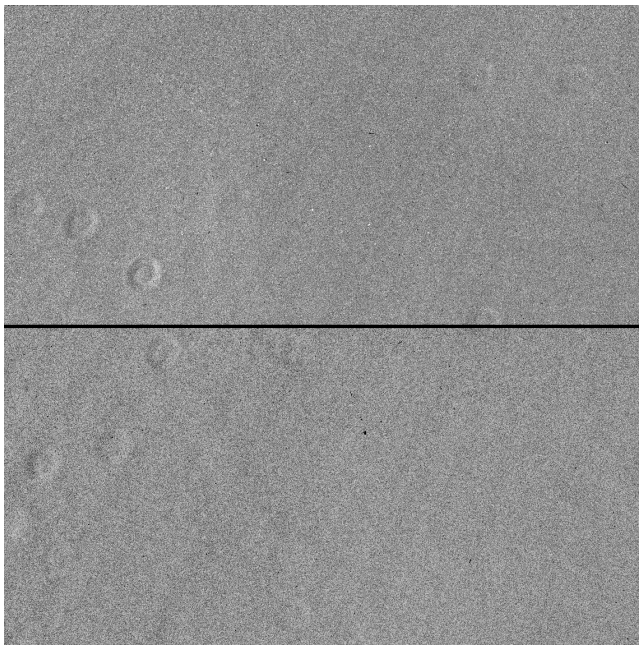

Fig. 2.—*Image ratio of a first and reference internal flat field showing ∼70-pixel wide dimple-like features (<1%) caused by inconsistent final positions of filter wheel 10 (F475X). Chip 1 (amps A and B) is shown in the top panel, while chip 2 (amps C and D) is shown in the bottom; greyscale stretch is +/-5%.*

Another nominal ratio feature is caused by variations in the travel speeds of the shutter blades. Hilbert 2010 shows through internal flat field observations that this 'shutter shading' causes a variation in exposure time across the detector of less than 0.001 seconds. These variations manifest themselves in the internal flat field ratios as faint, diagonal stripes that run from the lower left to the upper right corners of each chip, as shown in Figure 3. This striping is preferentially associated with the blade B shutter configuration; the ∼0.5% peak-to-peak features were seen in 52 of the 100 blade B SMOV visits, while all blade A SMOV data were flat to better than 0.2%. An inspection of post-SMOV data confirms that this behavior has not changed.

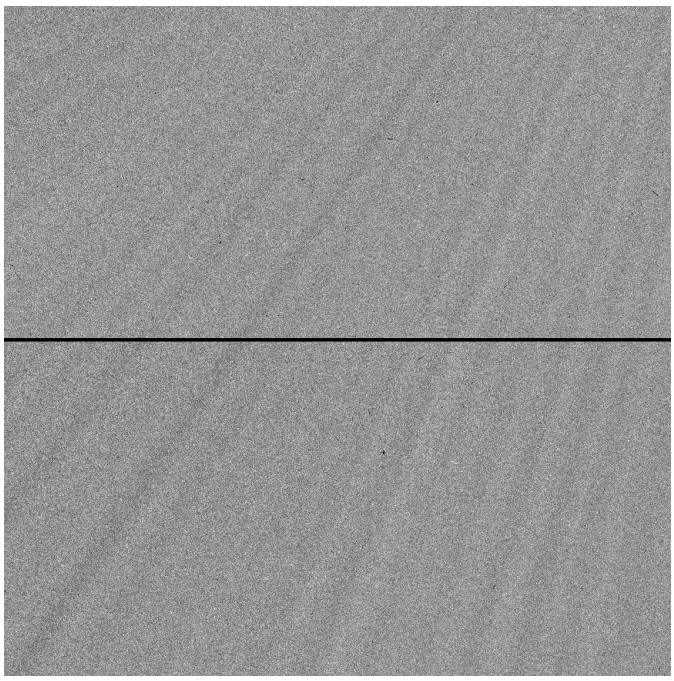

Fig. 3.—*Image ratio of a first and reference bowtie flat field showing diagonal stripe features caused by variations in shutter blade speed. Chip 1 (amps A and B) is shown in the top panel, while chip 2 (amps C and D) is shown in the bottom; greyscale stretch is +/-5%.*

Hysteresis-related Ratio Features

Two hysteresis-related ratio features are seen in bowtie observations; one is a typical feature which occurs after the UVIS anneal procedure (Figure 4), and the other is from an anomalous event wherein a bowtie-shaped feature was seen for the first (and only) time on-orbit (Figure 5). In bowtie visits occurring directly after the CCD is cooled down (typically UVIS anneals but early in the mission included Science Instrument Control and Data Handling Unit (SIC&DH) upsets), a prominent enhanced spot is seen in quadrant D (the thinnest part of the detector) accompanied by a deficit in quadrant C, with a peak-to-peak variation of ∼3%. Additionally, some faint cross-hatching is seen in quadrants A and B. An example of the usual post-anneal hysteresis is shown in the image 1/reference image ratio in Figure 4 (left). However, since each anneal procedure is followed by a bowtie QE 'pinning' exposure, this feature is successfully erased, as seen in the corresponding image 3/reference image ratio (Figure 4, right). Figure 6, which plots the average of rows 80-180 across the chips, shows further evidence of the ∼3% post-anneal feature. This feature and the global QE deficit do not show up in any other bowtie visits except immediately after the detectors are cooled down. Thus, the anneal-related hysteresis is completely removed and presents no risk to science or calibration observations between anneals.

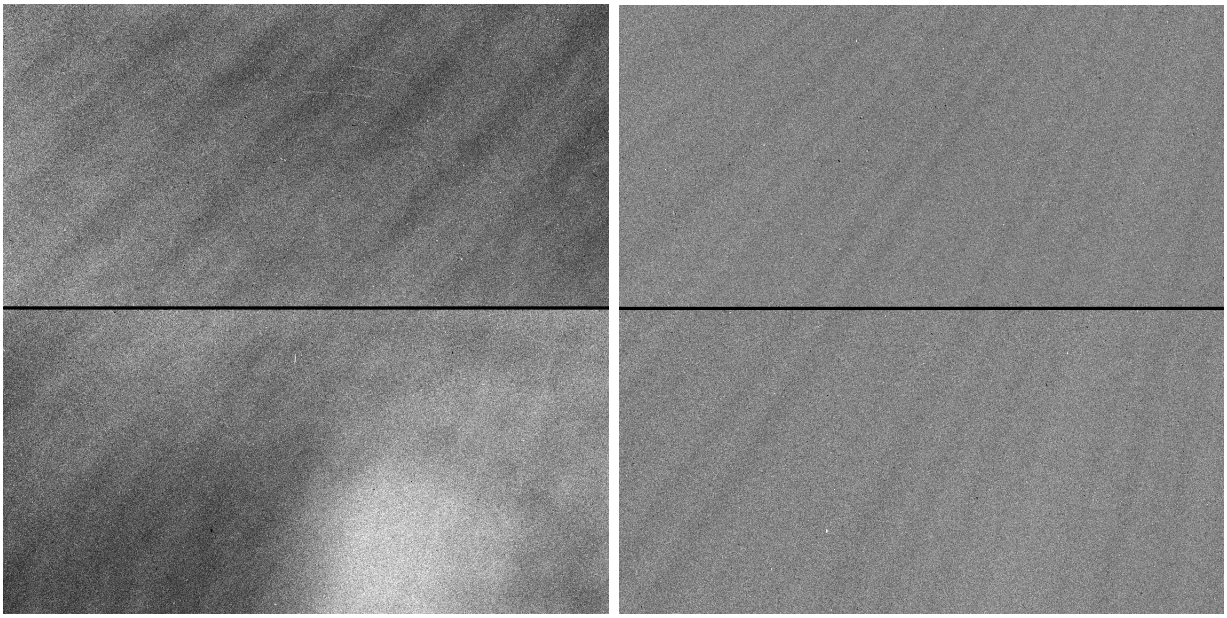

Fig. 4.—*An image 1/image 3 ratio (left, stretched to +/-5%) showing hysteresis caused by a UVIS anneal and the ratio of the image 3/reference bowtie image (right, stretched to +/-5%) from the same visit, showing that the hysteresis is erased by the saturated 'pinning' exposure. Chip 1 (amps A and B) is shown in the top panels, while chip 2 (amps C and D) is shown in the bottom.*

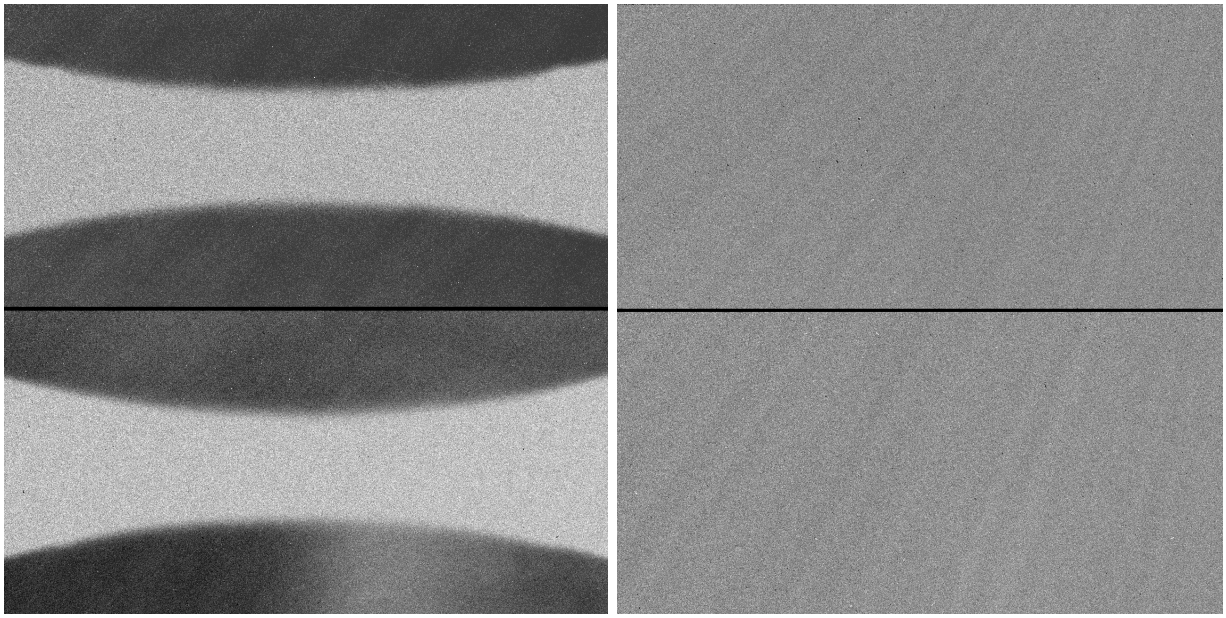

Fig. 5.—*Ratio of the image 1/image 3 from the bowtie visit directly after the August 2012 anneal (left, stretched to +/-5%), showing the bowtie-shaped hysteresis feature seen for the first time on-orbit, and the image 3/reference image from the same bowtie visit (right, stretched to +/-5%) showing that the hysteresis is erased by the saturated 'pinning' exposure. Chip 1 (amps A and B) is shown in the top panel, while chip 2 (amps C and D) is shown in the bottom panel.*

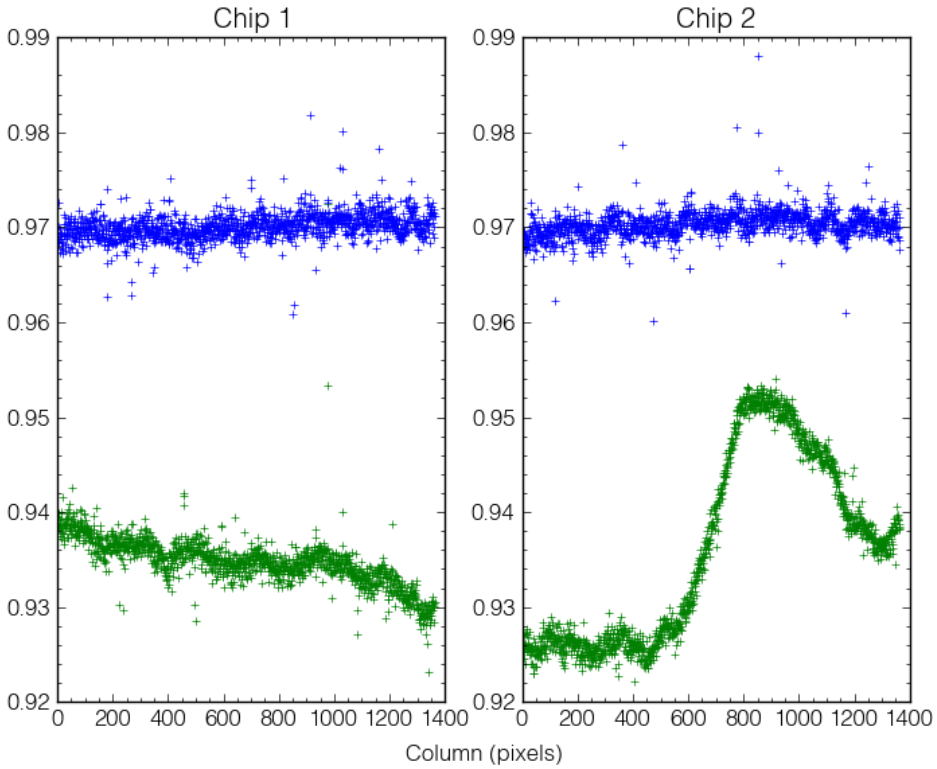

Fig. 6.—*Average of rows 80-180 for image 1/image 3 ratios for a nominal bowtie visit (blue) and a bowtie visit immediately following a UVIS anneal (green). Chip 1 (amps A and B) is shown in the left panel, while chip 2 (amps C and D) is shown in the right. The nominal visit shows about +/-0.2% peak-to-peak variation while the ∼3% QE feature is seen in the post-anneal bowtie visit.*

The bowtie visit that occurred directly after the August 2012 anneal saw a bowtie-shaped hysteresis feature for which the program was named, and has been the only occurrence of such a feature since ground testing. Figure 7 showcases this bowtie feature; it displays the average column values for all rows of each chip for (1) a nominal bowtie visit (blue), (2) a post-anneal bowtie visit (green), and (3) the post-August anneal bowtie visit (black). Note that the lamp is not completely warmed up during the first bowtie image in each visit, causing the nominal image1/image3 ratio levels to be ∼0.97 instead of 1.0. The cause of the anomalous bowtie shape is unknown. One possible contributor to the occurrence of the bowtie feature on-orbit could be the Flight Software (FSW) update that occurred in parallel to the August 2012 anneal procedure, wherein the UVIS detector and CCD Electronics Box (CEB) was power-cycled only about 10 minutes prior to the post-anneal bowtie visit, and the CEB temperatures were not yet stable. In addition to the FSW update, the anneal commanding and UVIS CCD temperature profile were also investigated, but appeared to have been nominal (Baggett et. al, 2013).

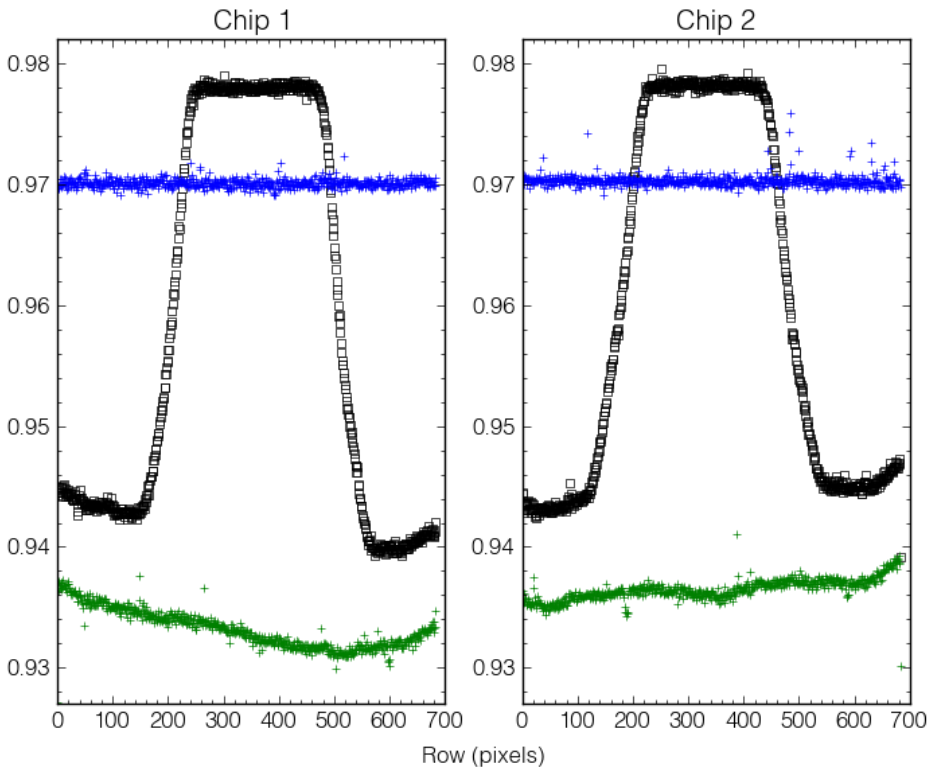

Fig. 7.—*Average of all columns for image 1/image 3 ratios for three types of bowtie visits. A nominal bowtie visit is shown in blue, where the image 1/image 3 ratios are nominally at 0.97 because the lamp is not completely warmed up for image 1. An example of a bowtie visit immediately following a UVIS anneal is shown in green, showcasing the global QE offset caused by the cooling of the detectors. Finally, the bowtie visit from the anomalous August 2012 anneal is shown in black. Chip 1 (amps A and B) is shown in the left panel, while chip 2 (amps C and D) is shown in the right.*

Despite this distinct hysteresis feature, the saturating bowtie exposure following the August 2012 anneal functioned as intended, as evident by the right panel of Figure 5, which shows that the feature has disappeared in the image 3/reference image ratio. Thus, the bowtie visit functioned as intended and no science or calibration data were affected by hysteresis.

Results

In order to detect any variations from the first bowtie image to the third bowtie image, median values were computed for each image ratio (image 1/reference, image 1/image 3, and image 3/reference) for each chip. The results are shown in Figures 8, 9, and 10, respectively, where chip 1 data are represented by Xs and chip 2 data are displayed as open circles. HST safing events caused by SIC&DH failures are represented as vertical red lines. During the first two SIC&DH

failures, the UVIS detector was warmed then cooled, which can cause hysteresis. However, since the October 22, 2009 (day 133) SIC&DH lockup, the WFC3 detectors have been kept cold during such events, but they remain plotted for consistency. Each anneal cycle is represented by alternating vertical grey and white regions (i.e. each grey/white border represents an anneal). Bowtie visits immediately following UVIS anneals have 3-4% lower signal levels than those from the bowtie monitoring programs, due to the QE deficit (Figures 8 and 9). Note that the normal image 1 to image 3 ratio in Figure 9 is not 1.0 but 0.97; this is due to the lamp not being completely warmed up during the first image of each bowtie visit. Further, note that the overall trend in Figure 9 does not match that of Figures 8 and 10. This is due to the fact that the image 1/image 3 trend does not reflect the time evolution of the lamp output, since the two images are from the same visit.

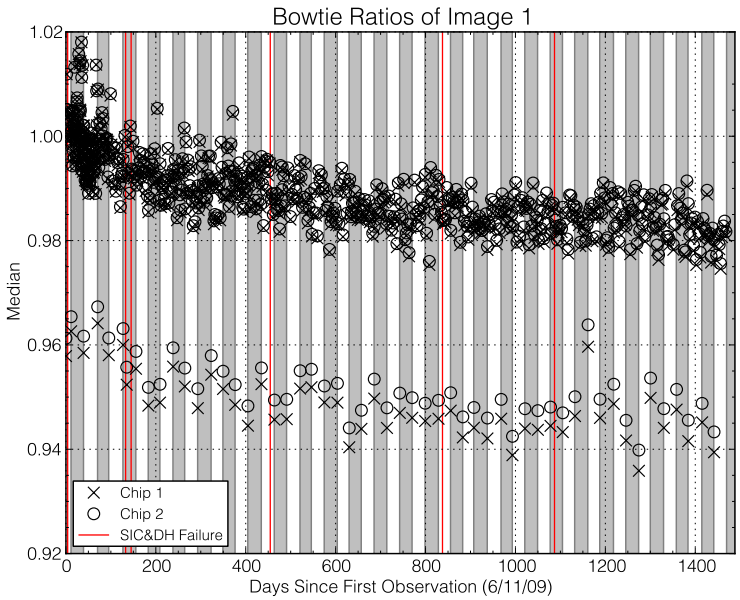

Fig. 8.—*Median levels of the ratio between bowtie image 1 and the reference image, as a function of days since the first observation. Each grey/white border represents a UVIS anneal. The vertical red lines indicate SIC&DH failures. Chip 1 median values are represented by Xs and chip 2 median values are represented by open circles.*

There exist several outlier data points in the plots (e.g. the high data point at day 371 and the low point at day 808 in Figure 8); these have been listed in Table 1 of Appendix A. The anomalous data points are likely attributable to lamp fluctuations. As Dahlen et al. 2013 show, the lamp intensity is stable to only about 0.4%. Calculating the median values of the image ratios after introducing this offset to the internal flat fields, we see that these lamp fluctuations place ± 0.005 error bars on each median value and establishes the outliers within the envelope of normal scatter expected due to lamp brightness fluctuations. In particular, several outliers exist in Figure 8, before day 50, in which median values exceed 1.0. The cause for these high ratios is unknown; they do not

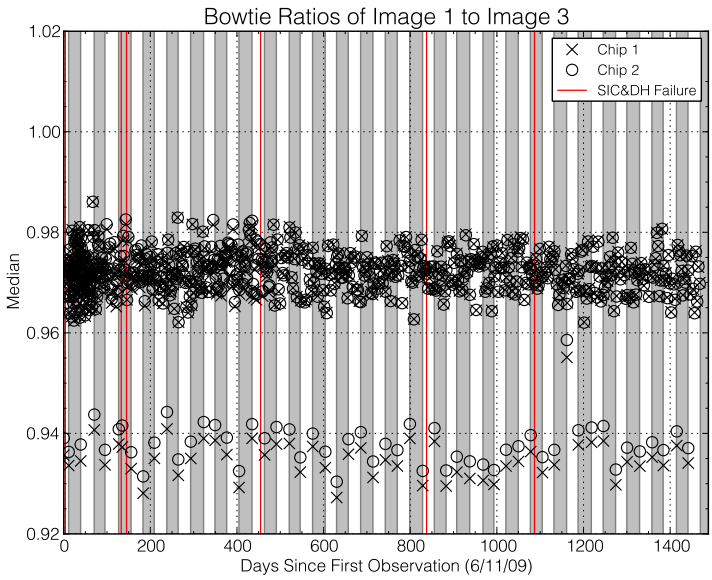

Fig. 9.—Median levels of the ratio between image 1 and image 3, as a function of days since first observation. Each grey/white border represents a UVIS anneal. The vertical red lines indicate SIC&DH failures. Chip 1 median values are represented by Xs and chip 2 median values are represented by open circles.

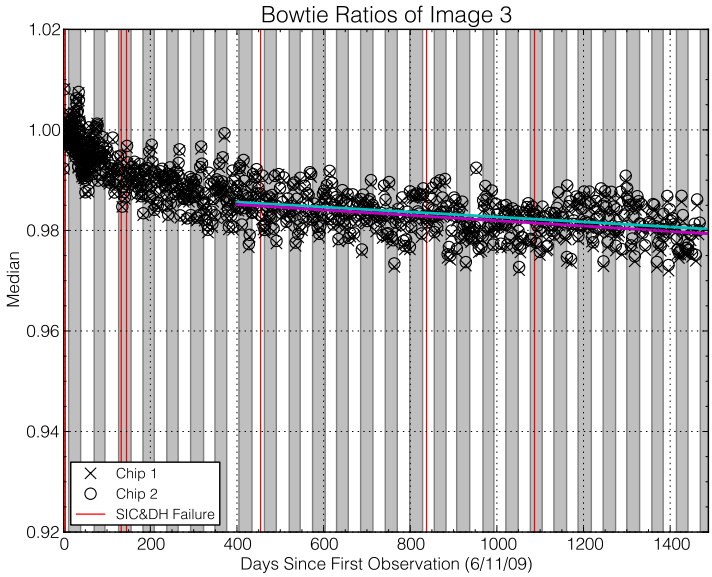

Fig. 10.—*Median levels of the ratio between image 3 and the reference image, as a function of days since first observation. Each grey/white border represents a UVIS anneal. The vertical red lines indicate SIC&DH failures. Chip 1 median values are represented by Xs and chip 2 median values are represented by open circles. A line of best linear fit is plotted for Chip 1 (magenta) and Chip 2 (cyan) data after day 400; lamp decline is ∼0.19±0.01%/year.*

appear to be an effect of a QE overshoot; though many internal flats were taken during these early stages of Cycle 17 via programs such as 11432 (UVIS Internal Flats) and 11428 (D2 Calibration Lamp Test), no internal flats taken within 10 hours before the bowtie visit appear to be oversaturated to a level known to cause a QE overshoot. Further investigation of the lamp behavior during the first few months on-orbit will be needed to understand the cause of these anomalous ratios. Nevertheless, the data from outlier visits in each ratio are always evaluated with additional checks of image ratios to nearby bowtie visit data, assessment of the global levels, and image histograms. Aside from the day 1161 (August 2012 anneal) anomalous data points in Figures 8 and 9, all outliers appear to be hysteresis-free.

In particular, the image 3/reference image ratio plot shown in Figure 10 reveals clues to the success of the hysteresis-quenching bowtie visits. Using a two-pronged approach of (1) identifying image 3/reference image ratio outliers beyond the 0.4% lamp fluctuation noise and (2) further investigating said outliers via visual inspection as well as by plotting their average row/column values (e.g. Figures 5 and 7), no evidence is seen of a hysteresis pattern to $\sim$0.2%. In addition, the effectiveness of the hysteresis quenching is reflected in the on-orbit photometric monitoring results which are stable to $<$0.5% (Kalirai et al., 2010; Hammer & Deustua, 2013). Though non-outliers are also inspected visually, it is conceivable that undetected hysteresis could exist at the sub-percent level, especially if no discernable features are present.

Finally, Figure 10 shows that the measured countrates are declining slowly over the long-term, which would be consistent with a slow decrease in lamp output. Early in the mission, the flux dropped about 1% over just $\sim$100 days; the decline has slowed significantly since then. For lamps like these, a decrease in output as they age is expected. Early prototypes of the tungsten bulbs tested on the ground showed dramatic declines in flux levels over timescales of only $\sim$1 month (Baggett, 2008). The current in-flight bulbs are the result of a significantly improved lamp design intended to provide longer useful lifetimes, a successful redesign given the more than 4 years of productive on-orbit operations to date. The lamp output as measured from internal flatfields in a variety of filters showed $\sim$0.5% decline over the first $\sim$60 days of on-orbit operations (Rajan & Baggett, 2010), in agreement with the decline seen in the first two months of bowtie data. These early images were acquired during a time period in which the lamps were heavily-used for on-orbit commissioning of the instrument, which we speculate might have contributed to the steeper decline in output. A fit to the data after day 400 indicates that the drop is $\sim$0.19$\pm$0.01%/year. Assuming the drop is solely due to a decline in lamp output, the lamp is now at $\sim$98% of its initial value.

Conclusion

Through ground-based lab tests, the WFC3/UVIS detector, along with similar e2v devices, were shown to exhibit occasional detector hysteresis. This effect can present itself in the form of a global QE offset or a bowtie-shaped pattern. The hysteresis can be effectively mitigated by overexposing the detector to several times the full well amount, thereby filling the traps that are

causing the issue. As a result, the on-orbit 'bowtie monitoring' program was adopted as a means to detect and neutralize UVIS hysteresis before it can adversely affect any science data. The routine bowtie monitors have been running successfully since WFC3 was installed in HST. Observations initially were taken at a cadence of twice per day but given the favorable on-orbit experience, have been reduced to once every three days.

Based on in-flight observations and consistency with the lab data, hysteresis has only been detected immediately after the detector has been warmed and then cooled back to operating temperature, as done for anneal procedures. None of the other bowtie visits between anneals have shown any evidence of hysteresis down to the ∼0.2% level. The characteristic hysteresis pattern on-orbit shows a global deficit of several percent across the field of view, along with slight cross-hatching in chip 1 (amps A and B) and a round area within amp D with somewhat higher QE. Only one of the 52 bowtie visits immediately following a UVIS anneal (August 2012) resulted in a bowtie-shaped feature for which the program was named. Results indicate that hysteresis mitigation has and continues to be successful; no anomalous image ratios are seen and ratio levels remain nominal. There is a slight long-term decline evident in the bowtie data, currently ∼0.19±0.01%/year; we speculate the drop may be due to a decline in lamp output, a common characteristic for lamps such as these. Bowtie monitoring is expected to continue through and beyond HST's 20th proposal cycle. For updated bowtie plots and documentation, please visit http://www.stsci.edu/hst/wfc3/ins_performance/monitoring/.

Acknowledgements

We would like to thank John Biretta for his thorough review of this ISR.

References

Baggett, S. and Richardson, M., TV1 Shift Report, August 29-30, 2004.

Baggett, S., "WFC3 TV2 Testing: Calibration Subsystem Performance," WFC3 Instrument Science Report 2008-01, January, 2008.

Baggett, S., and Borders, T., "WFC3 SMOV Proposal 11808: UVIS Bowtie Monitor," WFC3 Instrument Science Report 2009-24, January, 2010.

Baggett, S., Bourque, M., Biretta, J., Wheeler, T., Hickey, D., and Swain, S., "Anomalous Monitor Results After the Aug 2012 Anneal," WFC3 Technical Instrument Report 2013-01, March, 2013.

Collins, N. R., Boehm, N., Delo, G., Foltz, R. D., Hill, R. J., Kan, E., Kimble, R. A., Malumuth, E., Rosenberry, R., Waczynski, A., Wen, A., Baggett, S., Bushouse, H., Deustua, S., Kim-Quijano, J., MacKenty, J., Martel, A., and Sabbi, E., "Wide Field Camera 3 CCD Quantum Efficiency Hysteresis: Characterization and Mitigation," SPIE, August 2009, Volume 7439, 2009.

Dahlen, T., "WFC3/IR Internal Flat Fields," WFC3 Instrument Science Report 2013-04, March, 2013.

Hammer, D., and Deustua, S., "Photometric Stability of the WFC3," in prep., 2013.

Hilbert, B., "UVIS Channel Shutter Shading," WFC3 Instrument Science Report 2009-25, June, 2010.

Kalirai, J. S., Baggett, S., Borders, T., and Rajan, A., "The Photometric Performance of WFC3/UVIS: Temporal Stability Through Year 1," WFC3 Instrument Science Report 2010-14, October, 2010.

Rajan, A. and Baggett, S., "WFC3 SMOV Proposal 11432: UVIS Internal Flats," WFC3 Instrument Science Report 2010-03, January, 2010.

Appendix A: Anomalous Bowtie Image Ratios

Ratio	Rootname	Days since 6/11/09	Chip 1 Median	Chip 2 Median
image 1/reference	ibct88xaq	203.2	1.0052	1.0054
image 1/reference	ibct2uv3q	371.2	1.0041	1.0048
image 1/reference	ibld35nbq	586.3	0.9778	0.9783
image 1/reference	ibld94x9q	763.3	0.9770	0.9777
image 1/reference	ibld0jawq	808.5	0.9753	0.9760
image 1/reference	ibtxb3pkq*	1161.6	0.9597	0.9639
image 1/image 3	ibct09j3q/ibct09j5q	67.2	0.9861	0.9860
image 1/image 3	ibct0siyq/ibct0sj0q	263.3	0.9829	0.9829
image 1/image 3	ibct0tv2q/ibct0tv4q	265.3	0.9621	0.9621
image 1/image 3	ibld0jawq/ibld0jayq	808.5	0.9624	0.9624
image 1/image 3	ibtxb3pkq/ibtxb3pmq*	1161.6	0.9548	0.9583
image 1/image 3	ibu80pjeq/ibu80pjgq	1201.3	0.9618	0.9618
image 3/reference	ibct2uv5q	371.2	0.9986	0.9993
image 3/reference	ibld69eiq	688.3	0.9756	0.9762
image 3/reference	ibld94xbq	763.3	0.9727	0.9734
image 3/reference	ibu824h4q	928.3	0.9730	0.9737
image 3/reference	ibu832wgq	952.3	0.9920	0.9925
image 3/reference	ibu865xeq	1051.3	0.9721	0.9727
image 3/reference	ibu80fcvq	1171.4	0.9735	0.9743
image 3/reference	ic5la3wkq	1246.1	0.9729	0.9738
image 3/reference	ic4518hwq	1297.4	0.9899	0.9909
image 3/reference	ic4542fsq	1369.3	0.9727	0.9737
image 3/reference	ic4545puq	1378.3	0.9759	0.9770

Table 1: *Anomalous median values for bowtie image ratios, attributed to lamp fluctuations, or the August 2012 Anneal (as indicated by *).*